Time-resolved fluorescence polarization dynamics and optical imaging of Cytate: a prostate cancer receptor-targeted contrast agent

Y. Pu,[1,*] W. B. Wang,[2] B. B. Das,[2] S. Achilefu,[3] and R. R. Alfano[2]

[1]Institute for Ultrafast Spectroscopy and Lasers, and New York State Center for Advanced Technology for Ultrafast Photonic Materials and Applications, Department of Electrical Engineering, The City College of the City University of New York, Convent Avenue at 138th Street, New York, New York 10031, USA

[2]Institute for Ultrafast Spectroscopy and Lasers, and New York State Center for Advanced Technology for Ultrafast Photonic Materials and Applications, Department of Physics, The City College of the City University of New York, Convent Avenue at 138th Street, New York, New York 10031, USA

[3]Washington University School of Medicine, 4525 Scott Avenue, St. Louis, Missouri 63110, USA

*Corresponding author: puyang@sci.ccny.cuny.edu

Received 1 June 2007; revised 29 February 2008; accepted 14 March 2008; posted 27 March 2008 (Doc. ID 83626); published 25 April 2008

Cypate-octreote peptide analogue conjugate (Cytate) was investigated as a prostate cancer receptor-targeted contrast agent. The absorption and fluorescence spectra of Cytate were ranged in the near-infrared "tissue optical window." Time-resolved investigation of polarization-dependent fluorescence emitted from Cytate in solution as well as in cancerous and normal prostate tissues was conducted. Polarization preservation characteristics of Cytate in solution and tissues were studied. Fluorescence intensity emitted from the Cytate-stained cancerous prostate tissue was found to be much stronger than that from the Cytate-stained normal prostate tissue, indicating more Cytate uptake in the former tissue type. The polarization anisotropy of Cytate contained in cancerous prostate tissue was found to be larger than that in the normal prostate tissue, indicating a larger degree of polarization preservation in Cytate-stained cancerous tissue. The temporal profiles of fluorescence from Cytate solution and from Cytate-stained prostate tissue were fitted using a time-dependent fluorescence depolarization model. The photoluminescence imaging of Cytate-stained cancerous and normal prostate tissues was accomplished, showing the potential of Cytate as a fluorescence marker for prostate cancer detection.

OCIS codes: 300.6280, 110.3080.

1. Introduction

Prostate cancer was projected to account for ~29% of all cancer incidences in men, exceeding lung and bronchus cancer in the US, and to cause more than 27000 deaths in 2007 [1]. Currently prostate cancer diagnosis is based on digital rectal examination (DRE), blood prostate specific antigen (PSA) test, and the trans-rectal ultrasound (TRUS) imaging [2]. While TRUS is no longer considered as a first-line screening test for prostate cancer because of its poor spatial resolution and contrast [3], DRE has a reported sensitivity of as low as 18%–22% in asymptomatic men [2]. PSA has limited specificity, and the reported positive predictive value of PSA in asymptomatic men is 28%–35% [2]. The confirmation of prostate cancer requires a needle biopsy of the prostate. In the biopsy, a number of cores of prostate tissue are taken out with a thin needle guided into selectedregions of the prostate with an ultrasound probe. Because of poor spatial resolution and limited

0003-6935/08/132281-09$15.00/0

accuracy of these currently available methods, and the invasive nature of needle biopsy, there is a need to develop a noninvasive technique for early detection of prostate cancer with higher accuracy and resolution.

Fluorescence spectroscopy was used as a novel tool for detection of cancer by Alfano and his group [4] in the 1980s. The work was extended to differentiate human malignant breast tissues from benign and normal tissue types using UV excitation [5]. Further work on breast tissues and atherosclerotic arteries showed how time-resolved fluorescence could provide information not available from steady state spectral analysis alone [6]. Several groups have investigated various promising approaches using optical spectroscopy [7] and imaging [8] with high sensitivity and spatial resolution [3,7–10]. Since conventional steady state fluorescence measurements are performed by integrating fluorescence over a longer time in comparison with the lifetime of the fluorescence, the resulting data do not include information of the dynamics of the emission process and the effect of depolarization on fluorescence due to scattering in tissues. Some of these issues may be addressed by performing time-resolved fluorescence depolarization measurements, which measure the intensity profile and degree of polarization of fluorescence within its lifetime, and provide information complementary to that obtained from steady state spectral measurements [11].

The use of intrinsic chromophores to differentiate the optical properties of diseased and healthy human tissues is limited by their ultraviolet emission bands [12], which are far from the near-infrared (NIR) "tissue optical window" [13]. Over the past decade, Indocyanine Green (ICG, also called Cardio Green), a clinically approved NIR dye by the US Food and Drug Administration (FDA), has been investigated as a contrast agent for optical detection of tumors [14]. ICG fluoresces in the range of 775 nm to 850 nm, which avoids the absorption bands at 950 nm and 1195 nm due to water, which is the main chromophore component in human tissue in the NIR range [15,16]. However, ICG is not designed to specifically target cancer cells. The investigations of receptor expression in normal and cancer tissues suggest that small peptide-dye conjugates can be used to target over-expressed receptors on tumors to enhance specificity [17]. Biological studies have indicated that somatostatin receptors (SSTRs), which have five subtypes, are over-expressed in human prostate tumor [18]. It was reported that each subtype of somatostatin receptors could be identified on the basis of molecular modeling of its corresponding peptide conjugate [19]. The previous investigation showed that a small ICG-derivative dye-peptide, cypate-octreote peptide analogue conjugate (Cytate), could be used for effectively targeting somatostatin receptor-rich tumor in the animal model because of the high affinity of Cytate for the somatostatin receptors [20].

In this paper, we report time-resolved fluorescence and NIR imaging studies for Cytate, an optical contrast agent for human prostate cancer detection. The absorption and fluorescence spectra of Cytate were measured in the wavelength regions from 650 nm to 900 nm and 1100 nm, respectively. Time-resolved fluorescence polarization measurements were performed on Cytate solution and Cytate-stained cancerous and normal prostate tissues. Fluorescence imaging of two small pieces of Cytate-stained normal and cancerous prostate tissues (one for each) sandwiched between large pieces of normal prostate tissues was accomplished.

The experimental data obtained from a Cytate solution were fitted using a time-dependent fluorescence depolarization model [21,22]. The resultant parameters from Cytate fluorescence in solution and in prostate tissue were compared for understanding the effect of the rotational degree of freedom of Cytate in a tissue medium. An empirical model was applied to describe the time-resolved fluorescence kinetics and polarization anisotropy of Cytate in human prostate tissue. The differences of fluorescence and image intensities between Cytate-stained cancerous and normal prostate tissues showed preferential uptake of Cytate in the former tissue type.

2. Tumor-Targeted Mechanism of Cytate and Its Absorption and Fluorescence Spectra

Cytate used in this study was prepared by Achilefu's group at the Washington University School of Medicine. The molecular structure of Cytate is shown in Fig. 1. It is mainly composed of ICG and the somatostatin receptor ligand, which delivers the ICG to the receptors presented in the tumor [20]. The synthesis of this contrast agent was reported elsewhere [20]. The advantages of this receptor-targeted peptide-dye contrast agent include enhancing localization in tumors, rapid clearance from the nontarget (normal) tissue, possibility of preparing a library of peptides for rapid identification of bioactive molecules [20], and keeping the spectral advantages in

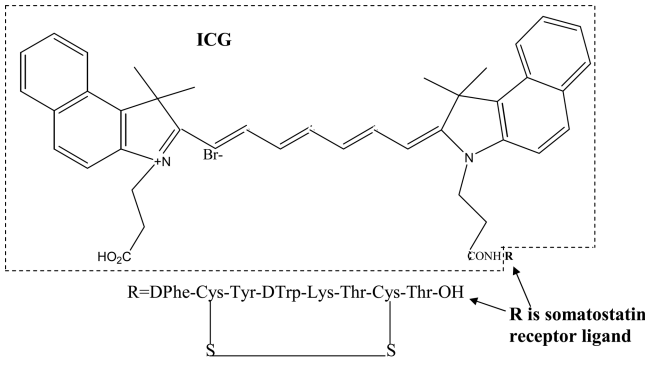

Cytate: Abbreviation of Cypate-Octreote Peptide Analogue Conjugate

Fig. 1. Molecular structure of the cypate-octreote peptide analogue conjugate (Cytate). The part enclosed by a dashed box is ICG (nonspecific dye without a SSTR ligand). R indicates the molecule chain of a SSTR ligand.

the NIR "tissue optical window." It was reported that the small ICG-derivative dye-peptide, Cytate, preferentially localized for over 24 hours in tumor with over-expressed somatostatin receptors in an animal model [20].

The human prostate is a highly hormone-sensitive organ. Numerous studies have found that somatostatin is directly or indirectly responsible in the regulation of prostate function [23]. Somatostatin is a small cyclic peptide. In addition to playing an important regulatory role of hormones, this peptide controls cell proliferation in cancerous tissues [18]. Therefore, tumors arising from somatostatin-needed tissues frequently express a high density of somatostatin receptors [24]. Somatostatin receptors are known for predominant expression in several human adenomas such as somatotroph and lactotroph adenomas, and neuroendocrine tumor including human prostate cancer [18,24,25], and can be used as a basis for *in vivo* tumor targeting. Several control experiments were carried out to determine whether expression of somatostatin receptors is up regulated in human prostate malignant cells [26]. Among them, Hansson *et al.* have found, by using fluorescing-labeled SSTR octreotide-binding probes by immunochemical analysis, that SSTR2 and SSTR4 are over-expressed in human prostate cancerous cells [26]. And Bugaj *et al.* have shown that the ligand of Cytate (ICG-derivative dye-peptide, cypate-octreote peptide analogue conjugate) to target somatostatin receptors in animal model is octreotide [20]. The combination of molecular probes and optical imaging methods has the potential to provide a better cancer detection technique with high sensitivity and specificity. The successful detection of Cytate in somatostatin receptors over-expressed in tumors in an animal model [20] motivated us to use Cytate to target the over-expressed specific SSTR2 and SSTR4 in human prostate cancerous cells. The basis of using Cytate as a prostate cancer contrast agent depends on two factors: (1) the high affinity of octreotide (ligand of Cytate) for the somatostatin receptors [20], and (2) the over-expression of SSTR2 and SSTR4 in human prostate cancer cells [26].

In our spectral study, Cytate was solvated in 20% aqueous dimethyl sulfoxide (DMSO). The absorption spectrum of Cytate in DMSO solution was measured using a Perkin-Elmer Lambda 9 UV/VIS/NIR spectrophotometer in the spectral range of 300 nm to 900 nm. The fluorescence spectrum of Cytate was measured using a far-red to NIR spectral setup excited by a 680 nm diode laser. Fluorescence emission from the sample was focused on the entrance slit of a SPEX Minimate 0.25 m monochromator (spectrometer) and detected by a Hamamatsu P394A PbS detector mounted at the exit slit of the monochromator. Signals from the detector were recorded by a PAR model HR-8 lock-in amplifier connected to a computer [27].

Figures 2(a) and 2(b) show the measured absorption and fluorescence emission spectra of Cytate,

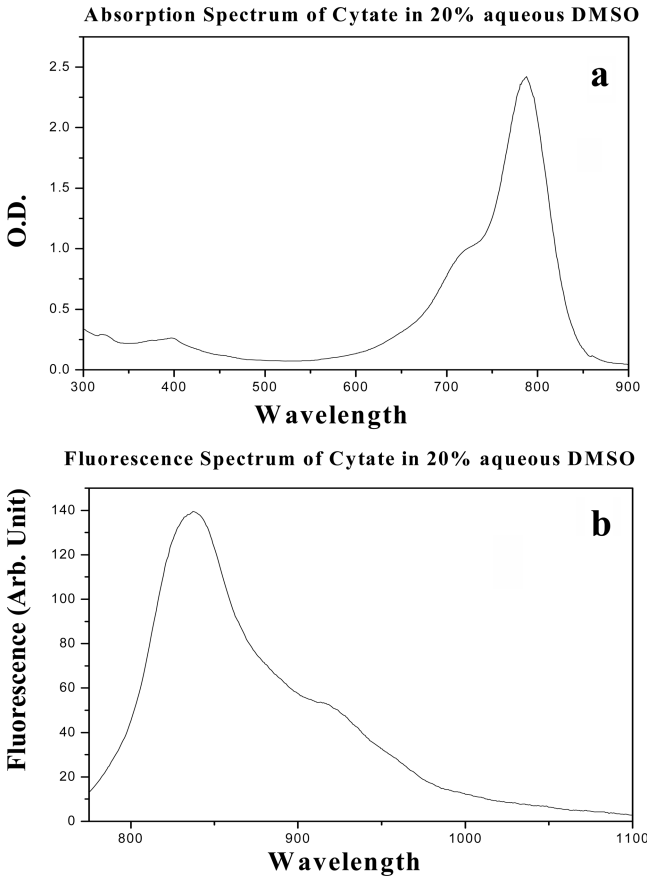

Fig. 2. (a) Absorption and (b) fluorescence spectra of Cytate in 20% aqueous DMSO. The fluorescence was obtained with an excitation of a 680 nm diode laser beam.

respectively. The absorption band of Cytate ranges from 680 nm to 830 nm with a shoulder peak at ~720 nm and a strong peak at 789 nm. The fluorescence spectrum covers from 800 nm to 950 nm with a main peak at 837 nm and a weak peak at 913 nm. The results show that Cytate possesses the spectral advantages of ICG, i.e., the fluorescence and the absorption ranges are in the NIR range of the "tissue optical window" [27].

3. Experimental Methods for Time-Resolved and Imaging Measurements

The experimental arrangement for the time-resolved fluorescence measurements is described in our previous work [10]. Pulses of 130 fs duration at 800 nm from a Coherent Mira 900 mode-locked Ti:sapphire laser at a repetition rate of 82 MHz were used to pump the samples (Cytate solution and Cytate-stained cancerous or normal prostate tissues). The fluorescence emission was collected by a large diameter lens with a focal length of 5 cm and directed onto the slit of a synchroscan streak camera with a temporal resolution of 10 ps. A long pass filter and an 800 nm notch filter were used to cut off the excitation wavelength. Two polarizers, P_1 and P_2, were used as a polarizer and an analyzer, respectively. The polarization direction of P_2 was varied

from 0° to 90° with respect to that of P_1 to record the fluorescence intensity profiles of parallel and perpendicular polarization components of the fluorescence. The temporal profiles recorded by a silicon intensified target (SIT) of the streak camera were analyzed to obtain temporal and polarization information [10].

The Cytate solution used for time-resolved fluorescence study was prepared by adding Cytate into 20% aqueous dimethyl sulfoxide (DMSO). Six cancerous and six normal prostate tissue samples from six different patients obtained from the National Disease Research Interchange (NDRI) and the Cooperation Human Tissue Network (CHTN) were used for the time-resolved fluorescence and optical imaging measurements under the Institutional Review Board (IRB) approval at City College of New York (CCNY). Each cancerous tissue had a corresponding normal tissue sample from the same patient used for the control experiment. Samples were neither chemically treated nor frozen prior to the experiments. Cancerous and normal prostate tissues used for the time-resolved fluorescence measurements were cut into ~2 cm × ~1 cm × ~0.5 cm (length × width × thickness) pieces. For each prostate tissue sample, measurements were performed at six different locations to get an average value. The cancerous and normal prostate tissue samples were soaked in the same Cytate-DMSO (20% aqueous dimethyl sulfoxide) solution with a Cytate concentration of $\sim 3.2 \times 10^{-6}$ M for fifteen minutes. Then the samples were put into sodium phosphate buffer (Sigma-Aldrich) to wash off the unbound Cytate. All the sample preparations and measurements were performed at room temperature.

The schematic diagram of the NIR optical imaging setup is shown in Fig. 3. A laser beam at 637 nm was used to illuminate the sample. A wide-bandpass filter at 800 nm with a FWHM of 40 nm was placed in front of a CCD camera to record images formed by light emitted from the sample. A bandpass filter was used to block the excitation wavelength and to collect only the light emitted from the sample. The spatial resolution of the CCD camera is 20 μm/pixel [10].

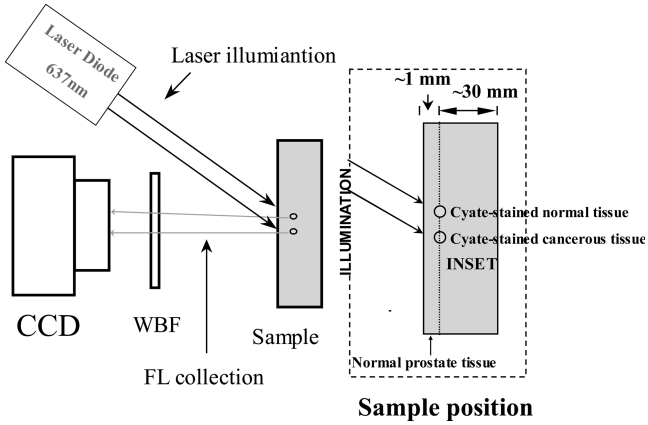

Fig. 3. Schematic diagram of the optical spectral imaging setup. The structure of a Cytate-stained cancerous-and-normal prostate tissue sample covered by a large piece of normal prostate tissue is shown schematically in the sample position.

The prostate tissue samples used for the imaging measurements consisted of a small piece of cancerous prostate tissue and a small piece of normal prostate tissue. They were first soaked in the same Cytate-DMSO (20% aqueous dimethyl sulfoxide) solution with a Cytate concentration of $\sim 3.2 \times 10^{-6}$ M for fifteen minutes, and then put into sodium phosphate buffer to wash off the unbound Cytate. The stained normal and cancerous prostate tissues were covered by a large piece of normal prostate tissue as shown in the sample position of Fig. 3.

4. Experimental Results and Discussion

A. Time-Resolved Fluorescence Polarization Anisotropy of Cytate in 20% Aqueous DMSO

The measured temporal profiles of the fluorescence emitted from Cytate in DMSO solution for two polarization directions, parallel and perpendicular to the polarization of the excitation at 800 nm, are shown in Fig. 4(a). The thick- and thin-curve profiles represent the parallel $[I_{\parallel}(t)]$ and perpendicular $[I_{\perp}(t)]$ components, respectively. The time-dependent polarization anisotropy can be calculated using the following equation [21,22]:

$$r(t) = \frac{I_{\parallel}(t) - I_{\perp}(t)}{I_{\parallel}(t) + 2I_{\perp}(t)}. \quad (1)$$

The thin curve in Fig. 4(b) displays the time evolution of $r(t)$ as calculated. The decay behavior of $r(t)$ reflects the dipole reorientation of Cytate in solvent since the degree of polarization of the fluorescence depends on the rotation time and fluorescence lifetime of the molecules [21,22]. If molecular rotation is much faster compared to the florescence lifetime, the emitting molecules become randomly oriented very quickly, resulting in depolarized emission. If molecules rotate much more slowly in comparison with the fluorescence decay time, then the emission remains strongly polarized. Polarization anisotropy found in our case suggests that rotation time is of the same order as fluorescence lifetime.

In Fig. 4(a), the main differences between parallel and perpendicular components are the following: (1) The intensity of $I_{\parallel}$ is greater than that of $I_{\perp}$ for all decay times. The peak intensity of the parallel component $I_{\parallel}(0)$ is almost three times stronger than that of the perpendicular component $I_{\perp}(0)$. This indicates the polarization preservation nature of Cytate. (2) There is a distinct difference between the decay slopes of the two components, which can be seen clearly by normalizing the peak of the perpendicular component to that of the parallel component, as shown by the thin-dashed curve in Fig. 4(a). Since the rotation time and fluorescence lifetime of Cytate are on same time scale in our case, the overall decay time is affected by both reorientation of molecules and fluorescence decay kinetics. Since the parallel

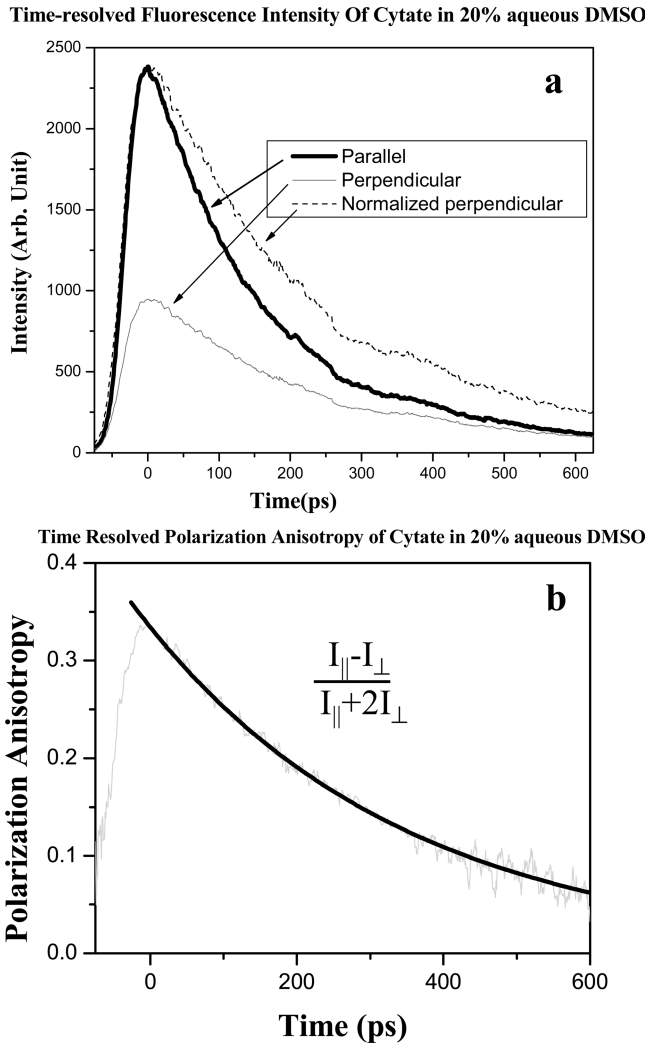

Fig. 4. Temporal polarization profiles and polarization anisotropy of light emitted from Cytate in 20% aqueous DMSO with a polarized 800 nm laser illumination. (a) Profiles of the time-resolved fluorescence components having polarization directions parallel (thick curve) and perpendicular (thin curve) to the polarization direction of the exciting light. The thin-dashed curve displays the normalized perpendicular components. (b) Time-dependent polarization anisotropy (thin curve) calculated using the measured data shown in (a) and Eq. (1) shown in the text, and the fitting curve (thick curve) calculated using Eq. (2) shown in the text and the data shown by the thin curve in Fig. 5(b).

and perpendicular components emitted from Cytate have same fluorescence lifetime, the fast decay of the parallel component and slow decay of the perpendicular component are caused by the Cytate molecular rotation.

In this simple model where Cytate molecules in solution are considered to undergo Brownian rotation as Einstein spheres, the time-resolved fluorescence kinetics and polarization anisotropy from Cytate in aquatic DMSO can be shown as [21,22]

$$r(t) = r(0)\,\exp\left(-\frac{t}{\tau_{\mathrm{rot}}}\right), \qquad (2)$$

where $r(0)$ is anisotropy at $t = 0$ and τ_{rot} is the rotation time of the fluorophore molecule in solvent, determined by the diffusion coefficient, the solvent viscosity, and the molecular radius [21,22]. The value of $r(0)$ depends on the angle between the absorption and emission dipoles, and the expectation value of the second order Legendre polynomial for the distribution function of dipoles [10,28]. The maximum theoretical value of $r(0)$ is 0.4 [10,21,22,28].

The experimental value of $r(0)$ obtained from the data shown in Fig. 4(b) is ~0.33, which is in reasonable agreement with the theoretical value of 0.4 [21,22]. As mentioned by Flemming [21] and Porter [22], the measured value of $r(0)$ is always smaller than its theoretical value due to (1) the rapid internal motions of the macromolecules, since the macromolecules must contain a flexible substructure that can undergo rapid depolarization rotation, (2) scattering of light in tissues, and (3) birefringence of the quartz cell containing the samples. This result indicates that the transition dipole moments of Cytate molecules in solution are randomly oriented, and the depolarization effects of Cytate in 20% aqueous DMSO solvent can be confined to molecular rotations and to the trivial effect of initial randomness [21]. The polarization anisotropy peak value, $r(0)$, and the rotation time,τ_{rot}, of Cytate in solution can be obtained by fitting the experimental data of $r(t)$ shown in Fig. 4(b) using Eq. (2). The best fit was obtained with the parameter values of $r(0) = 0.337 \pm 0.032$ and $\tau_{\mathrm{rot}} = 352 \pm 21$ ps, and the fitting curve is shown by the thick-dark curve in Fig. 4(b).

B. Time-Resolved Fluorescence Polarization Anisotropy of Cytate Contained in Stained Cancerous and Normal Prostate Tissues

Six Cytate-stained cancerous and six Cytate-stained normal prostate tissue samples from six patients were used for the time-resolved fluorescence measurements. For each sample, measurements were performed on six or more different locations for statistical analysis. Before the measurements were performed, the tissue sample was carefully checked to determine the hard parts to locate the small region of the cancerous tissue. This is acknowledged to be a simple way to find the location of malignancy [29]. Two typical time-resolved fluorescence intensity profiles for the cancerous and normal prostate tissue samples stained with Cytate are displayed in Fig. 5(a). The thick-solid and thick-dashed curve profiles represent the parallel and the perpendicular components of emission from stained cancerous tissue, respectively. The thin-solid and thin-dashed curve profiles display the parallel and perpendicular components of emission from stained normal tissue, respectively.

One of the most important features of the profiles in Fig. 5(a) is the higher emission intensity of the stained cancerous tissue compared to the stained normal tissue throughout the Cytate emission range. Using the data in Fig. 5(a), for the

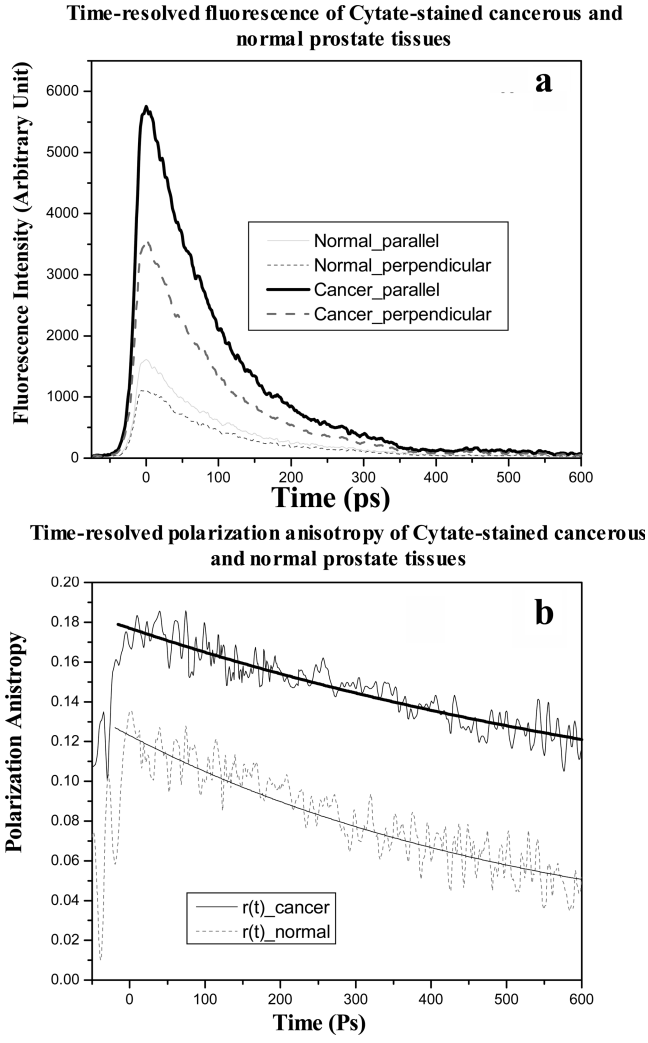

Fig. 5. (a) Time-resolved fluorescence intensity of light emitted from Cytate-stained cancerous and normal prostate tissues with 800 nm laser illumination. The thick-solid and thick-dashed curve profiles are the parallel and perpendicular components emitted from Cytate-stained cancerous prostate tissue, respectively. The thin-solid and thin-dashed curve profiles display the parallel and perpendicular components emitted from Cytate-stained normal prostate tissues, respectively. (b) Time-dependent polarization anisotropy calculated using Eq. (1) shown in the text and the measured data shown in Fig. 5(a). The thin-solid and thin-dashed curve profiles indicate the $r(t)$ for Cytate-stained cancerous and normal prostate tissues, respectively. The fitting curves for Cytate in cancerous prostate tissue (thick-solid curve) and Cytate in normal prostate tissue (thin-solid curve) were calculated using Eq. (3) shown in the text and the corresponding polarization anisotropy shown in Fig. 5(b).

parallel polarization configuration, the ratio of peak fluorescence intensity of the Cytate-stained cancerous tissue to that of the normal tissues was found to be ~3.57, while for the perpendicular configuration, the ratio was ~3.25. These ratios indicate that cancerous prostate tissue has higher Cytate intake than normal tissue.

Another important feature of the temporal profiles is that $I_{\parallel}$ is greater than $I_{\perp}$ throughout the decay period for both cancerous and normal tissues. At the peak position, $I_{\parallel}^{\text{cancer}}(0)$ is ~1.60 times stronger than $I_{\perp}^{\text{cancer}}(0)$, and the ratio of $I_{\parallel}^{\text{normal}}(0)$ to $I_{\perp}^{\text{normal}}(0)$ is ~1.46. This indicates that the fluorescence emitted from both Cytate-stained cancerous and normal prostate tissues show the polarization preservation property, although the ratio of $I_{\parallel}(0)/I_{\perp}(0)$ is smaller than that of Cytate solution. Using Eq. (1) and the measured values of $I_{\parallel}(t)$ and $I_{\perp}(t)$ shown in Fig. 5(a), the temporal profiles of the polarization anisotropy $r(t)$ from Cytate in stained cancerous (thin-solid curve) and normal (thin-dashed curve) prostate tissues were calculated, and the results are displayed in Fig. 5(b).

The interesting features of $r(t)$ curves shown in Fig. 5(b) are the following: (1) the profiles of Cytate-stained tissue show a flatter decay compared to that of Cytate solution; and (2) the values of the polarization anisotropy of Cytate in the stained cancerous tissue are always larger than that of the stained normal tissue. The peak intensity values of $r(0)$ for cancerous and normal tissues were found to be $r(0)^{\text{cancer}} = 0.167 \pm 0.021$ and $r(0)^{\text{normal}} = 0.133 \pm 0.011$, presented as mean values $\pm$ standard deviations. These results indicate that the Cytate-stained cancerous tissue shows a better polarization preservation property than the Cytate-stained normal prostate tissue. The polarization preservation properties of Cytate-stained prostate tissue can be used to enhance the image contrast between cancerous and normal prostate tissue areas combining with a fluorescence-polarization-difference imaging (FPDI) technique [10,27,30].

The value of $r(0)$ for a dye solution depends on the viscosity of the solvent [28]. Above a critical value of the viscosity of about 3000 poise, a normalized orientation distribution function was used as a model for fluorescent molecules instead of random distribution [28]. By applying this distribution function, a value of $r(0) = 0.1039$ was calculated for the condition of the viscosity greater than 3000 poise [10,28]. It was also reported that biological living tissue might mimic the behavior of viscous liquids [31]. The viscosities of biological tissues, including prostate tissue, were reported to be much higher than 3000 poise [32]. If the case of Cytate in prostate tissue is considered as a fluorescent dye in a "very high viscosity liquid," the anisotropy $r(0)$ should be expected to be in the range between ~0.10 and ~0.12.

The physical model generated from our previous study [10] on cybesin (another NIR contrast agent used to target bombesin receptor that is also overexpressed in prostate tumors) suggests that the time-resolved fluorescence polarization anisotropy $r(t)$ of the emission from NIR fluorescent dye contained in stained human prostate tissues can be considered to have two components: (1) a static anisotropy component caused by the emission from the tissue cell-bonded Cytate molecules without rotation; and (2) a time-dependent anisotropy component formed by the emission from the unbound Cytate

molecules with rotation in the body fluid of prostate tissue [10]. These assumptions are reasonable because a tissue cell is too massive to rotate compared to a Cytate molecule. This empirical model was developed to describe the time-resolved fluorescence kinetics and polarization anisotropy emitted from contrast agent stained tissues [10]. Using this model, the temporal fluorescence polarization anisotropy $r(t)$ of Cytate contained in stained prostate tissues can be described by

$$r(t) = r_1 + r_0 \exp\left(-\frac{t}{\tau_{\text{rot}}}\right), \tag{3}$$

where $r_0 \exp(-t/\tau_{\text{rot}})$ is the time-dependent portion of the polarization anisotropy induced by the "free" Cytate molecules in the fluid of prostate tissue, τ_{rot} is the rotation time of the "free" Cytate in prostate tissue, $r(0)$ is the peak value of the polarization anisotropy of the "free" Cytate molecules, and r_1 is the static portion of the polarization anisotropy induced by the cell-bond Cytate molecules in prostate tissue. The three parameters τ_{rot}, r_0, and r_1 can be obtained by fitting the experimental data of $r(t)$ shown in Fig. 5(b) using Eq. (3).

The best fitting curves for Cytate-stained cancerous (thick-solid curve) and normal (thin-solid curve) prostate tissues are shown in Fig. 5(b). The fitting results yielded the following parameters: $r_0 = 0.115 \pm 0.012$, $\tau_{\text{rot}} = 900 \pm 180$ ps, and $r_1 = 0.062 \pm 0.013$ for Cytate in stained cancerous prostate tissue, and $r_0 = 0.109 \pm 0.030$, $\tau_{\text{rot}} = 550 \pm 140$ ps, and $r_1 = 0.014 \pm 0.004$ for Cytate in stained normal tissue. These values are in reasonable agreement with our experimental data.

The fitting results yield that $r_1^{\text{cancer}} > r_1^{\text{normal}}$. This can be understood from the fact that the perpendicular component of the fluorescence emitted from cell-bond Cytate molecules is mainly contributed by the photons undergoing multiple scattering [10,30]. Since the excitation wavelength of 800 nm is close to the strong absorption peak of Cytate and cancerous prostate tissue has higher Cytate intake than normal tissue, the stained cancerous tissue region would absorb more photons than the stained normal tissue regions. Light from the same excitation source would go deeper in normal prostate tissue than in cancerous tissue. As a result, the fluorescence from normal prostate tissue comes from the Cytate molecules embedded in deeper tissue layers than the Cytate molecules in the cancerous prostate tissue [10]. The light emitted from the stained cancerous tissue area undergoes less multiple scattering than that from the stained normal tissue. As a result, the degree of polarization and the value of r_1 for the stained cancerous tissue region are much larger than that of the stained normal tissue region [10].

The fitting results also show that $\tau_{\text{rot}}^{\text{cancer}} > \tau_{\text{rot}}^{\text{normal}}$. The larger decay time of free Cytate molecules in cancerous prostate tissue indicates the higher local viscosity of cancerous prostate tissue due to high density and decreasing interstitial spacing between cells. The higher density of cancerous cells can be recognized by the nature of evolution of a malignant tumor [29]. First the tumor grows in volume; when it reaches some kind of confining volume, the mechanical pressure increases its cell density. When the tumor cell density exceeds a certain compaction maximum, invasion starts [29,33]. The tumor grading system for prostate cancer includes the well known five Gleason grades, usually denoted as stages 1–5 [34]. The pattern of Gleason grade 1 (corresponding to early stage) consists of a circumscribed mass of evenly placed uniform glands. With grade advances, the cancer cells proliferate and begin to merge into an "island" [34]. This pattern appears at grade 3 and is obvious at grade 5 [34]. The microscopic histological images shown in our previous work [27] also indicate the "island" structure and high density of cancerous cell. The higher cell density in cancerous prostate tissue [29,33,34] gives the molecules less "free" rotation space [10,29,34]. In addition, the dye crowds more in cancerous tissue due to higher adsorption levels of bound Cytate as shown by the larger emission intensity in Fig. 5(a). The crowding dye chains form a compact or contracted coil in which the dye is embedded [35]. This effect increases the local viscosity [35], which in our view is the reason behind the larger decay time of Cytate in cancerous prostate tissue compared to that in normal prostate tissue samples.

5. Optical Imaging

To study the potential of Cytate for prostate cancer detection by NIR imaging, cancerous-and-normal prostate tissue samples were imaged using a NIR spectral imaging system. In order to image a hidden tissue, a small piece of cancerous prostate tissue and another small piece of normal prostate tissue stained with Cytate were sandwiched between two large pieces of prostate normal tissue with a thickness of ~1 mm for the front piece. The fluorescence images of the Cytate-stained prostate tissues were recorded at 800 nm by exciting at 637 nm. Figure 6(a) shows recorded NIR images of the stained cancerous and normal prostate tissues embedded underneath the ~1 mm thick normal prostate tissues. As displayed in Fig. 6(a), the emission intensity of the Cytate-stained cancerous tissue is higher than that of the Cytate-stained normal tissue.

This property of preferential uptake of Cytate by cancerous prostate tissue can be more clearly visualized by Fig. 6(b), which is the digital spatial cross section of intensity distribution of the image shown in Fig. 6(a). Using the digital data shown in Fig. 6(b), the ratio of imaging intensity of the cancerous tissue area to that of normal tissue area is found to be ~3.54. To compare the results of the imaging measurements with that of time-resolved fluorescence experiments, peak intensities of $I_{\parallel}$ and $I_{\perp}$ for both cancerous and normal tissue shown in Fig. 5(a) were added, and the ratio of peak fluorescence intensities emitted from Cytate-stained cancerous tissue to that

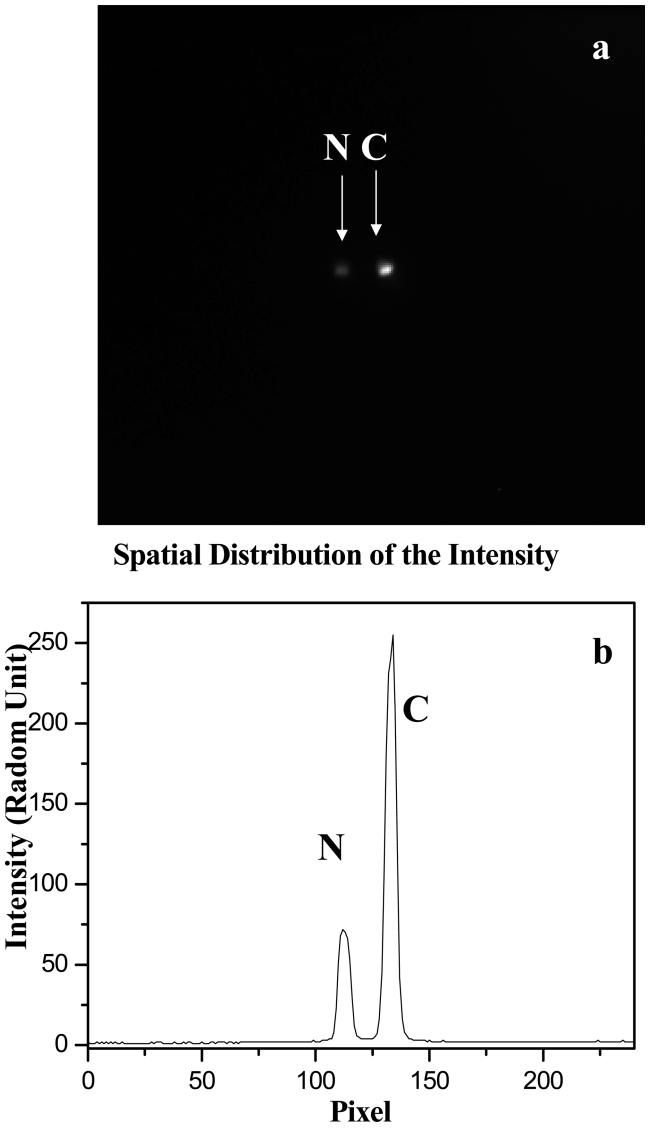

Fig. 6. (a) Contrast agent fluorescence image of a cancerous-and-normal prostate tissue sample (a tiny piece of Cytate-stained cancerous prostate tissue and a tiny piece of Cytate-stained normal prostate tissue covered by a large piece of normal prostate tissue). (b) Digital spatial cross section intensity distribution of the image shown in Fig. 6(a) at a row crossing the areas of the stained cancer (C) and normal (N) tissues.

from the normal tissue was calculated to be ~3.45. This value obtained from the time-resolved fluorescence measurements is in a good agreement with that obtained from the spectral imaging measurements.

Both fluorescence intensity measurements and optical spectral imaging study show the preferential uptake of Cytate by prostate cancerous tissue. Since Hansson *et al.* reported that the over-expressed SSTR2 and SSTR4 on prostate tumor cells bind octreotide [26], and the ligand of Cytate to target somatostatin receptors in animal model is octreotide [20], we may infer that Cytate achieved targeting the over-expressed specific SSTR2 and SSTR4 in human prostate cancerous cells.

6. Conclusion

Steady state absorption- and fluorescence-spectral measurements were performed on Cytate, a cancer receptor-targeted contrast agent, to study its viability in cancer detection. Time-resolved fluorescence kinetics and polarization anisotropy of Cytate in solution and in stained human cancerous and normal prostate tissues were investigated. The experimental results show a larger degree of polarization preservation of fluorescence from Cytate in the stained cancerous tissue than in the stained normal tissue. The fluorescence intensity emitted from the Cytate-stained cancerous prostate tissue was found to be much stronger than that from the Cytate-stained normal prostate tissue indicating that cancerous prostate tissue has a higher Cytate intake than normal tissue. The time-resolved fluorescence intensity profile from a Cytate solution was fitted using a time-dependent fluorescence depolarization model. An empirical physical model was applied to describe the behavior of fluorescence kinetics and polarization anisotropy of Cytate in stained cancerous and normal prostate tissues. Optical imaging of cancerous and normal prostate tissues stained with Cytate was performed. The fluorescence image of the Cytate-stained cancerous prostate tissue region was found to be much brighter than that of the Cytate-stained normal tissue region. Cytate was shown to be an excellent contrast agent because its absorption and fluorescence spectra lie in the NIR "tissue optical window." Both fluorescence intensity and optical imaging studies show the potential of Cytate as a fluorescent marker in prostate cancer detection.

7. Future Work

Further biomedical studies are needed to follow up this spectral and optical imaging investigation. Some immunochemical analysis is needed to identify the somatostatin receptor subtypes that are targeted by Cytate. Experiments for quantifying the difference in the number of somatostatin receptors between cancerous and normal prostate tissues need to be performed and compared for different Gleason grades. Some biomedical work is needed to study the transport of Cytate across the cell membrane and into the cell cytoplasm, and to see whether 20% DMSO concentration of aqueous solution has any adverse effect on tissue.

This research is supported by U.S. Army Medical Research and Material Command under grant DAMD17-01-1-0084 (CUNY RF 47462-00-01). The authors acknowledge the help of NDRI and CHTN for providing normal and cancerous prostate tissue samples for the measurements, the valuable discussion with G. C. Tang at IUSL and C. J. Gu at Molecular Virology Division of Columbia University Medical Center, and the help of M. Sharanov at IUSL for the Cytate fluorescence spectrum measurements.

References

1. A. Jemal, R. Siegel, E. Ward, T. Murray, J. Xu, and M. J. Thun, "Cancer statistics, 2007," CA Cancer J. Clin. **57**, 43–66 (2007).
2. R. Ferrini and S. H. Woolf, "Screening for prostate cancer in American men: American College of Preventive Medicine practice policy statement," http://www.acpm.org/prostate.htm
3. D. A. Benaron, "The future of cancer imaging," Cancer Metastasis Rev. **21**, 45–78 (2002).
4. R. R. Alfano, D. Tata, J. Cordero, P. Tomashefsky, F. Lonyo, and M. Alfano, "Laser induced fluorescence spectroscopy from native cancerous and normal tissue," IEEE J. Quantum Electron. **20**, 1507–1511 (1984).
5. R. R. Alfano, B. B. Das, J. B. Cleary, R. Prudente, and E. Celmer, "Light sheds light on cancer: distinguishing malignant tumor from benign tissues and tumors," Bull. N.Y. Acad. Med. **67**, p. 143 (1991).
6. B. B. Das, Feng Liu, and R. R. Alfano, "Time-resolved fluorescence and photon migration studies in biomedical and model random media," Rep. Prog. Phys. **60**, 227 (1997)
7. I. J. Bigio and J. R. Mourant, "Ultraviolet and visible spectroscopies for tissue diagnosis," Phys. Med. Biol. **42**, 803–814 (1997).
8. S. Kumar and R. Richards-Kortum, "Optical molecular imaging agents for cancer diagnostics and therapeutics," Nanomedicine **1**, 23–30 (2006).
9. A. Villringer and B. Chance, "Noninvasive optical spectroscopy and imaging of human brain function," Trends Neurosci. **20**, 435 (1997).
10. Y. Pu, W. B. Wang, S. Achilefu, B. B. Das, G. C. Tang, V. Sriramoju, and R. R. Alfano, "Time-resolved fluorescence polarization anisotropy and optical imaging of Cytate in cancerous and normal prostate tissues," Opt. Commun. **274**, 260–267 (2007).
11. K. Vishwanath, B. Pogue, and M.-A. Mycek, "Quantitative fluorescence lifetime spectroscopy in turbid media: comparison of theoretical, experimental and computational methods," Phys. Med. Biol. **47** 3387–3405 (2002).
12. K. C. Smith, *The Science of Photobiology*, 2nd ed. (Plenum, 1989).
13. D. J. Dean and B. J. Korte, "Biomedical imaging and bioengineering," Opt. Photon. News (October 2003), http://ultra.bu.edu/papers/2003_10_OPN.pdf.
14. L. Kai, B. Riefke, V. Ntziachristos, A. Becker, B. Chance, and W. Semmler, "Hydrophilic cyanine dyes as contrast agents for near-infrared tumor imaging: synthesis, photophysical properties and spectroscopic *in vivo* characterization," Photochem. Photobiol. **72**, 392–398 (2002).
15. G. M. Hale and M. R. Querry, "Optical constants of water in the 200 nm to 200 mm wavelength region," Appl. Opt. **12**, 555–563 (1973).
16. J. H. Ali, W. B. Wang, M. Zevallos, and R. R. Alfano, "Near infrared spectroscopy and imaging to probe differences in water content in normal and cancer human prostate tissues," Technol. Cancer Res. Treat. **3** 491–497 (2004).
17. B. Ballou, G. W. Fisher, J. S. Deng, T. R. Hakala, and M. Srivastava , "Cyanine fluorochrome-labeled antibodies *in vivo*: assessment of tumor imaging using Cy3, Cy5, Cy5.5 and Cy7," Cancer Detect. Prev. **22**, 251–257 (2000).
18. J. C. Reubi, B. Waser, J. C. Schaer, and R. Markwalder, "Somatostatin receptors in human prostate and prostate cancer," J. Clin. Endocrinol. Metabol. **80**, 2806–2814 (1995).
19. S. P. Rohrer, E. T. Birzin, R. T. Mosley, and S. C. Berk, "Rapid identification of subtype-selective agonists of somatostatin receptor through combined chemistry," Science **282**, 737–740 (1998).
20. J. E. Bugaj, S. Achilefu, R. B. Dorshow, and R. Rajagopalan, "Novel fluorescent contrast agents for optical imaging of *in vivo* tumor based on a receptor-targeted dye-peptide conjugate platform," J. Biomed. Opt. **6**, 122–133 (2001).
21. G. R. Fleming, J. M. Morris, and G. W. Robinson, "Direct observation of rotational diffusion by picosecond spectroscopy," Chem. Phys. **17**, 91–100 (1976).
22. G. Porter, P. J. Sadkowski, and C. J. Tredwell, "Picosecond rotational diffusion in kinetic and steady state fluorescence spectroscopy," Chem. Phys. Lett. **49**, 416–420 (1977).
23. A. V. Schally, "Oncological applications of somatostatin analogs," Cancer Res. **48**, 6977–6985 (1988).
24. L. J. Hofland and S. W. J. Lamberts, "Somatostatin subtype expression in human tumors," Ann. Oncol. **12** (2), 31–36 (2001)
25. E. Thodou, G. Kontogeorgos, D. Theodossiou, and M. Pateraki, "Mapping of somatostatin receptor types in GH or/and PRL producing pituitary adenomas," J. Clin. Pathol. **59**, 274–279 (2006).
26. J. Hansson, A. Bjartell, V. Gadaleanu, N. Dizeyi, and P. Abrahamsson, "Expression of somatostatin receptor subtypes 2 and 4 in human benign prostatic hyperplasia and prostatic cancer," Prostate **53**(4), 50–59 (2002).
27. Y. Pu, W. B. Wang, G. C. Tang, F. Zeng, S. Achilefu, J. H. Vitenson, I. Sawczuk, S. Peters, J. M. Lombardo, and R. R. Alfano, "Spectral polarization imaging of human prostate cancer tissue using a near-infrared receptor-targeted contrast agent," Technol. Cancer Res. Treat. **4**, 429–436 (2005).
28. F. Pellegrino, "Energy transfer in the primary stages of the photosynthetic process investigated by picosecond time resolved fluorescence spectroscopy," Ph.D. dissertation (City University of New York, 1981), pp. 270–315.
29. A. Shmilovici, "Incomplete tumor volume reduction may improve cancer prognosis," Med. Hypoth. **68**, 1236–1239 (2007).
30. W. B. Wang, S. G. Demos, J. Ali, and R. R. Alfano, "Imaging fluorescence objects embedded inside animal tissue using a polarization difference technique," Opt. Commun. **142**, 161–166 (1997).
31. D. A. Beysens, G. Forgacs, and J. A. Glazier, "Cell sorting is analogous to phase ordering in fluids," Proc. Natl. Acad. Sci. USA **97**, 9467–9471 (2000).
32. M. A. Dresner, P. J. Rossman, S. A. Kruse, and R. L. Ehman, "MR elastography of the prostate," ISMRM 99 CDs http://cds.ismrm.org/ismrm-1999/PDF2/526.pdf.
33. T. S. Deisboeck, Y. Mansury, C. Guiot, P. G. Degiorgis, P. Giorgio, and P. P. Delsanto, "Insights from a novel tumor model: indications for a quantitative link between tumor growth and invasion," Med. Hypoth. **65**, 785–790 (2005).
34. D. F. Gleason and G. T. Mellinger, "Prediction of prognosis for prostate adenocarcinoma by combined histological and clinical prostatic staging," J. Urol. **111**, 58–64 (1974).
35. H. P. M. de Oliveira and M. H. Gehlen, "Time resolved fluorescence anisotropy of basic dyes bound to poly(methacrylic acid) in solution," J. Braz. Chem. Soc. **14**, 738–743 (2003).